nature portfolio

https://doi.org/10.1038/s41567-022-01700-1

Supplementary information

Zero-field superconducting diode effect in small-twist-angle trilayer graphene

In the format provided by the authors and unedited

Supplementary Materials: zero-field superconducting diode effect in small-twist-angle trilayer graphene

Jiang-Xiazi Lin, Phum Siriviboon, Harley D. Scammell, Song Liu, Daniel Rhodes, K. Watanabe, T. Taniguchi, James Hone, Mathias S. Scheurer, and J.I.A. Li†

† Corresponding author. Email: jia_li@brown.edu

This PDF file includes:

SI 1: Symmetry analysis for superconducting diode effect

Let us begin with a discussion of general constraints on the superconducting diode effect based on symmetry. Denoting the magnitude of the maximum current density the superconductor can support along the in-plane direction $\hat{n}$ by $J_c(\hat{n})$, the supercurrent diode effect is defined by

$$\exists\hat{n}: \quad \delta J_c(\hat{n}) := J_c(\hat{n}) - J_c(-\hat{n}) \neq 0. \tag{S1}$$

Since the current direction is odd under time-reversal and under two-fold out-of-plane rotation or three-dimensional inversion symmetry, the presence of at least one of these symmetries implies that

$$J_c(\hat{n}) = J_c(-\hat{n}) \tag{S2}$$

and no diode effect can be present. In turn, the observation of a finite diode effect in our sample unambiguously demonstrates that all three of these symmetries must be broken in the superconducting state.

There are two qualitatively different ways for this to happen, which are in principle consistent with our observations: (i) all three of these symmetries are already broken in the normal state out of which superconductivity emerges or (ii) at least one of these symmetries is broken spontaneously when (the magnitude) of the superconducting order parameter becomes finite. As already discussed in the main text, we believe that option (ii) is less natural since the underlying pairing must be unconventional; we therefore focus on (i) in the following and refer to [1] for more details on (ii).

In Table SI, we list the point symmetries of mirror-symmetric twisted trilayer graphene, as a function of whether a displacement field D_0 is applied, Rashba, $\lambda_{\rm R}$, or Ising, $\lambda_{\rm I}$, spin-orbit coupling is present, and whether there is strain, β, in the samples. For completeness, we also list their representation on the continuum-model field operators $(\psi_{\boldsymbol{k};\ell,\boldsymbol{G}})_{\rho,\eta,s}$ with s denoting the spin, ρ the sublattice, and η the valley quantum number (and the associated Pauli matrices are denoted by s_j, ρ_j, and η_j); ℓ labels the two mirror even $\ell = 1, 2$ and the mirror-odd, $\ell = 3$, layer wavefunctions (see [1–3] where the same conventions are used), and $\boldsymbol{G}$ are vectors of the reciprocal moiré lattice. Note that we list both spinless forms of the symmetries (e.g., C_{2z}), which are only possible in the absence of spin-orbit coupling, and spinfull versions (C_{2z}^s or $C_{2z}^{s'}$), where the spatial transformations are combined with appropriate spin transformations. Importantly, the constraint in Eq. (S2) follows when any one of the spinfull or spinless forms of these symmetries, i.e., any of Θ, Θ^s, C_{2z}, C_{2z}^s, and $C_{2z}^{s'}$, are present.

While spin-orbit coupling breaks all two-fold rotational symmetries, Θ^s is always preserved (which also holds when further spin-orbit terms, like Kane-Mele-type spin-orbit coupling, or a sublattice imbalance term, $m\rho_z$, that could be induced by WSe_2, are taken into account). In scenario (i) introduced above, the normal state above the superconducting transition temperature must therefore exhibit spontaneously broken time-reversal symmetry, induced by electronic interactions. Furthermore, the associated particle-hole order parameter must coexist with superconductivity. We next discuss a few natural microscopic candidate forms for this symmetry-breaking order.

TABLE SI. Action of the point symmetries on the microscopic field operators ($\psi_{\boldsymbol{k}}$) of a continuum-model description of twisted trilayer graphene, using the same notation as in [1–3]. For convenience of the reader, we also list redundant symmetries. Here β is a parameter that describes strain-induced C_{3z}-symmetry breaking and $\lambda_{\rm R}$ ($\lambda_{\rm I}$) denotes Rashba (Ising) spin-orbit coupling.

Symmetry S	unitary	$S\psi_{\boldsymbol{k};\ell,\boldsymbol{G}}S^\dagger$	condition
$\mathrm{SO}(3)_s$	✓	$e^{i\boldsymbol{\varphi}\cdot\boldsymbol{s}}\psi_{\boldsymbol{k};\ell,\boldsymbol{G}}$	$\lambda_{\rm R} = \lambda_{\rm I} = 0$
$\mathrm{SO}(2)_s$	✓	$e^{i\varphi s_z}\psi_{\boldsymbol{k};\ell,\boldsymbol{G}}$	$\lambda_{\rm R} = 0$
C_{3z}	✓	$e^{i\frac{2\pi}{3}\rho_3\eta_3}\psi_{C_{3z}\boldsymbol{k};\ell,C_{3z}\boldsymbol{G}}$	$\lambda_{\rm R} = \beta = 0$
C_{3z}^s	✓	$e^{i\frac{2\pi}{3}(\rho_3\eta_3+s_3)}\psi_{C_{3z}\boldsymbol{k};\ell,C_{3z}\boldsymbol{G}}$	$\beta = 0$
C_{2z}	✓	$\eta_1\rho_1\psi_{-\boldsymbol{k};\ell,-\boldsymbol{G}}$	$\lambda_{\rm R} = \lambda_{\rm I} = 0$
C_{2z}^s	✓	$s_3\eta_1\rho_1\psi_{-\boldsymbol{k};\ell,-\boldsymbol{G}}$	$\lambda_{\rm I} = 0$
$C_{2z}^{s'} = C_{2z}^s i s_{2,1}$	✓	$s_{1,2}\eta_1\rho_1\psi_{-\boldsymbol{k};\ell,-\boldsymbol{G}}$	$\lambda_{\rm R} = 0$
σ_h	✓	$(1,1,-1)_\ell\psi_{\boldsymbol{k};\ell,\boldsymbol{G}}$	$D_0 = \lambda_{\rm R} = \lambda_{\rm I} = 0$
$I = C_{2z}\sigma_h$	✓	$\eta_1\rho_1(1,1,-1)_\ell\psi_{-\boldsymbol{k};\ell,\boldsymbol{G}}$	$D_0 = \lambda_{\rm R} = \lambda_{\rm I} = 0$
Θ	✗	$\eta_1\psi_{-\boldsymbol{k};\ell,-\boldsymbol{G}}$	$\lambda_{\rm R} = \lambda_{\rm I} = 0$
Θ^s	✗	$is_2\eta_1\psi_{-\boldsymbol{k};\ell,-\boldsymbol{G}}$	—

Different normal state orders. The first type of order parameter breaking time-reversal symmetry is spin magnetism. The associated three-component order parameter, $\boldsymbol{S}$, couples to the electrons according to

$$\Delta H_S = \sum_{\boldsymbol{k}\in \mathrm{MBZ}} \sum_{\boldsymbol{G}\in \mathrm{RML}} \sum_{\ell=1}^{3} g_{\ell,\boldsymbol{G}}(\boldsymbol{k})\, \psi^\dagger_{\boldsymbol{k};\ell,\boldsymbol{G}} \boldsymbol{s} \psi_{\boldsymbol{k};\ell,\boldsymbol{G}} \cdot \boldsymbol{S}, \tag{S3}$$

where MBZ (RML) denotes the moiré Brillouin zone (reciprocal moiré lattice), $\boldsymbol{s} = (s_x, s_y, s_y)$ are Pauli matrices in spin space, and $g_{\ell,\boldsymbol{G}} \in \mathbb{R}$ with $g_{\ell,\boldsymbol{G}}(\boldsymbol{k})$ only constrained by C_{2z} $[g_{\ell,\boldsymbol{G}}(\boldsymbol{k}) = g_{\ell,-\boldsymbol{G}}(-\boldsymbol{k})]$ and C_{3z} $[g_{\ell,\boldsymbol{G}}(\boldsymbol{k}) = g_{\ell,C_{3z}\boldsymbol{G}}(C_{3z}\boldsymbol{k})]$. Among the symmetries in Table SI of the model without spin-orbit coupling and strain, $\lambda_\mathrm{I} = \lambda_\mathrm{R} = \beta = 0$, non-zero $\boldsymbol{S}$ in Eq. (S3) only breaks $\mathrm{SO}(3)_s$ (down to the group of residual spin-rotations along the direction of $\boldsymbol{S}$). In the presence of any finite subset of λ_I, λ_R, β, additional symmetries are broken, with important consequences for the diode effect, as detailed below.

Note that in the presence of λ_I or λ_R, the spin-rotation symmetry $\mathrm{SO}(3)_s$ is broken (down to $\mathrm{SO}(2)_s$ or completely). Therefore, out-of-plane spin magnetization, $\boldsymbol{S} = (0, 0, S_z)$, and in-plane magnetization, $\boldsymbol{S} = (S_x, S_y, 0)$, are symmetry inequivalent and, hence, constitute physically distinct order parameters; we will thus analyze the diode effect for these two types of orientations of $\boldsymbol{S}$ separately below.

Before discussing that, though, let us introduce the second class of time-reversal-symmetry-breaking order, which is spontaneous valley polarization, V_z, with coupling

$$\Delta H_V = \sum_{\boldsymbol{k}\in \mathrm{MBZ}} \sum_{\boldsymbol{G}\in \mathrm{RML}} \sum_{\ell=1}^{3} \tilde{g}_{\ell,\boldsymbol{G}}(\boldsymbol{k})\, \psi^\dagger_{\boldsymbol{k};\ell,\boldsymbol{G}} \eta_z \psi_{\boldsymbol{k};\ell,\boldsymbol{G}} \cdot V_z, \tag{S4}$$

where η_z is the third Pauli matrix in valley space and $\tilde{g}_{\ell,\boldsymbol{G}}(\boldsymbol{k})$ is constrained exactly in the same way as g above. A finite valley polarization, $V_z \neq 0$, breaks both time-reversal and two-fold-rotation symmetry (along with inversion I) at the same time, as immediately follows from the representations in Table SI.

Consequences for diode effect. Using the symmetry criteria defined above, it is straightforward to determine whether a diode effect is allowed for the three different types of normal state orders—in-plane ($S_{x,y}$), out-of-plane (S_z) spin magnetization, and valley (V_z) polarization—in the presence or absence of spin-orbit coupling and strain. The result is summarized in the third column of Table SII. The findings imply, for instance, that the diode effect in case of out-of-plane spin magnetism has to be proportional to both S_z and the Ising-spin-orbit coupling strength, $\delta J(\hat{n}) \propto S_z\lambda_\mathrm{I}$; this simply follows from the fact that S_z alone (or combined with Rashba spin-orbit coupling or β) does not break C^s_{2z} and, therefore, does not allow for a diode effect. Similarly, we have $\delta J(\hat{n}) \propto S_{x,y}\lambda_\mathrm{R}$ for in-plane spin magnetism, as Rashba spin-orbit coupling is required to break $C^{s'}_{2z}$. In case of valley polarization, this is different as it breaks all two-fold rotational symmetries (and time-reversal) even without any spin-orbit coupling and, hence, $\delta J(\hat{n}) \propto V_z \neq 0$ even when $\lambda_\mathrm{I} = \lambda_\mathrm{R} = \beta = 0$.

Note that V_z and S_z are, from a pure symmetry perspective, equivalent as long as $\lambda_\mathrm{I} \neq 0$, while $S_{x,y}$ is still distinct; one important qualitative difference between out-of-plane spin polarization, S_z, or valley polarization, V_z, being responsible for the anomalous diode effect as compared to in-plane spin polarization, $S_{x,y}$, is that the diode effect for the latter will not be C_{3z} symmetric: as can be seen in the third and fourth column of Table SII, whenever we have a diode effect for $S_{x,y}$, which happens as long as $\lambda_\mathrm{R} \neq 0$, the critical current will not be C_{3z} symmetric, $J_c(\hat{n}) \neq J_c(C_{3z}\hat{n})$. This means that the current asymmetry, $\delta J_c(\hat{n}) := J_c(\hat{n}) - J_c(-\hat{n})$, is constrained to have at least two zeros when $\hat{n}$ rotates by 2π. This is different for S_z or V_z; as long as strain is negligible, $\beta = 0$, it holds $J_c(\hat{n}) = J_c(C_{3z}\hat{n})$ and consequently $\delta J_c(\hat{n})$ must have at least six zeros. Unless strain is sufficiently large, the number of sign changes will not be affected by $\beta \neq 0$.

By the same token, the response of the superconductor to an applied in-plane magnetic field $\boldsymbol{B} = (B_x, B_y, 0) = |\boldsymbol{B}|\hat{b}$, e.g., as reflected in its critical temperature, will display different angular dependence: T_c will be a (an approximately) C_{3z} symmetric function as long as $\beta = 0$ (β is small) for V_z and S_z, while it will not be invariant under a C_{3z} rotation of the magnetic field, see fifth column in Table SII, if $S_{x,y}$ causes the diode effect. This could be used to further check the order parameter underlying the diode effect in future experiments.

Field training. Another aspect that can be used to distinguish between the different candidate orders is whether they can be trained by in- and out-of-plane magnetic fields. Formally, we classify an order parameter $O \in \{S_z, S_{x,y}, V_z\}$ as trainable by a field $\mathcal{B}$ if a linear coupling $c\,O\mathcal{B}$ is allowed by the symmetries of the bare Hamiltonian (in turn depending on which of $\lambda_\mathrm{I}, \lambda_\mathrm{R}, \beta$ are non-zero) without the order O or $\mathcal{B}$. In the last four columns of Table SII, we list under which conditions this is possible for the three different orders and considering orbital and Zeeman coupling separately.

TABLE SII. We list for three different candidate orders of the normal state—out-of-plane spin polarization (S_z), in-plane spin polarization ($S_{x,y}$), and valley polarization (V_z)—whether a supercurrent diode effect, $J_c(\hat{n}) \neq J_c(-\hat{n})$, is allowed, depending on which of the three parameters, Rashba, λ_R, and Ising, λ_I, spin-orbit coupling, and strain, β, are non-zero. We further indicate whether the directional dependence of the critical current shows a free-fold rotation symmetry and whether the critical temperature of the superconductor is unaffected by rotating an applied magnetic field by C_{3z}. Finally, the last four columns indicated whether it can be trained by an in-plane (out-of-plane) Zeeman field $B^Z_\parallel$ ($B^Z_\perp$) or orbital magnetic field $B^O_\parallel$ ($B^O_\perp$). Throughout, we assume that the superconductor does not spontaneously break any additional point symmetry. Note that all results hold for both $D_0 = 0$ and $D_0 \neq 0$.

normal state		superconductor			trainable by			
parent order	non-zero terms	$J_c(\hat{n}) \neq J_c(-\hat{n})$	$J_c(\hat{n}) = J_c(C_{3z}\hat{n})$	$T_c(\hat{b}) = T_c(C_{3z}\hat{b})$	$B^Z_\perp$	$B^Z_\parallel$	$B^O_\perp$	$B^O_\parallel$
S_z	—	✗	✓	✓	✓	✗	✗	✗
	λ_R	✗	✓	✓	✓	✗	✓	✗
	λ_I	✓	✓	✓	✓	✗	✗	✗
	$\lambda_\mathrm{R}, \lambda_\mathrm{I}$	✓	✓	✓	✓	✗	✓	✗
	$\lambda_\mathrm{R}, \lambda_\mathrm{I}, \beta$	✓	✗	✗	✓	✓	✓	✓
$S_{x,y}$	—	✗	✓	✗	✗	✓	✗	✗
	λ_R	✓	✗	✗	✗	✓	✗	✓
	λ_I	✗	✓	✗	✗	✓	✗	✗
	$\lambda_\mathrm{R}, \lambda_\mathrm{I}$	✓	✗	✗	✗	✓	✗	✓
	$\lambda_\mathrm{R}, \lambda_\mathrm{I}, \beta$	✓	✗	✗	✓	✓	✓	✓
V_z	—	✓	✓	✓	✗	✗	✗	✗
	λ_R	✓	✓	✓	✗	✗	✗	✗
	λ_I	✓	✓	✓	✓	✗	✗	✗
	$\lambda_\mathrm{R}, \lambda_\mathrm{I}$	✓	✓	✓	✓	✗	✓	✗
	$\lambda_\mathrm{R}, \lambda_\mathrm{I}, \beta$	✓	✗	✗	✓	✓	✓	✓

Most importantly, $S_{x,y}$ can only be trained by an out-of-plane magnetic field if there is finite strain, $\beta \neq 0$, Rashba and Ising spin-orbit coupling $\lambda_\mathrm{R}, \lambda_\mathrm{I} \neq 0$. As such, the coupling strength $c \propto \beta\lambda_\mathrm{R}\lambda_\mathrm{I}$ is expected to be rather weak. In particular, much smaller than the coupling strength and, hence, trainability of $S_{x,y}$ with respect to in-plane magnetic fields, which does not require any of λ_I, λ_R, β to be non-zero (for the Zeeman part). This is the exact opposite of what is seen in experiment, where the diode effect can be efficiently trained with an out-of-plane magnetic field of order 25 mT, while it is much more difficult to train it with in-plane magnetic field (for those in-plane fields, of order 10 T, where we seem to have achieved training of the diode effect, the lower bound on the simultaneously applied out-of-plane field is also of order of 10 mT).

Instead, the observed behavior is consistent with either V_z or S_z since both can be trained by an out-of-plane Zeeman field (with the only difference that V_z further requires λ_I which is not small) but can only be trained by an in-plane field if β and λ_R are non-zero. Taken together, our measurements indicate that either V_z or S_z are the most natural candidate order parameters. We reiterate that, as long as λ_I is non-zero, as is the case for our system, it is not possible to distinguish between these remaining two options by symmetry; in fact, their order parameters are in the same irreducible representation of the high-temperature symmetry group such that they formally describe the same phase. Intuitively, this can be seen by noting that Ising spin-orbit coupling has the form $\lambda_\mathrm{I} s_z \eta_z$ such that a finite valley polarization will induce a spin-polarization along the spin-z axis, and vice versa.

SI 2: Absence of diode effect from in-plane field and Pauli limit violation

Due to the spin-orbit coupling induced in our sample by WSe_2, one might expect that the mechanism discussed in [4–6] for in-plane Zeeman fields and Rashba spin-orbit coupling, motivated by experiments [7] in artificial metal films, should apply here as well. This mechanism is based on the observation that an in-plane magnetic field will move Rashba spin-orbit-split Fermi surfaces in opposite directions leading to finite momentum pairing [8, 9] and a diode effect [4–6]. However, as can be seen in Fig. S7d, this is not the case in our experiments; as we will detail below, we expect this to result from the rather different nature of the spin-orbit coupling in our system.

To demonstrate this, let us focus on Ising spin-orbit coupling (setting $\lambda_\mathrm{R} = 0$); the inclusion of Rashba spin-orbit coupling is addressed in [1]. Only keeping the low-energy bands around the Fermi surface, with field operators $f^\dagger_{\boldsymbol{k},\eta,s}$

creating an electron at momentum $\boldsymbol{k}$, in valley η, and of spin s, an effective Hamiltonian reads as

$$H_{\rm LE} = \sum_{\boldsymbol{k},s,\eta} f^\dagger_{\boldsymbol{k},\eta,s} \left(\epsilon_{\eta\cdot\boldsymbol{k}} + \Gamma_{\rm I}(\boldsymbol{k};\eta)(s_z)_{s,s'}\,\eta + B_x(s_x)_{s,s'}\right) f_{\boldsymbol{k},\eta,s'} + \sum_{\boldsymbol{k}} \left[f^\dagger_{\boldsymbol{k},+,s}(\Delta_{\boldsymbol{k}})_{s,s'} f^\dagger_{-\boldsymbol{k},-,s'} + \text{H.c.}\right] + \delta H_{\rm LE}. \quad \text{(S5)}$$

Here $\Delta_{\boldsymbol{k}} = (\Delta^s_{\boldsymbol{k}} s_0 + \boldsymbol{d}_{\boldsymbol{k}} \cdot \boldsymbol{s})\, is_y$ is the superconducting order parameter, B_x an in-plane magnetic field (along x without loss of generality), and $\delta H_{\rm LE}$ are interaction terms, which we will not further have to specify and only assume that they preserve the, for superconductivity crucial [10], enhanced $\text{SU}(2)_+{\times}\text{SU}(2)_-$ spin symmetry. Finally, $\Gamma_{\rm I}(\boldsymbol{k};\eta)$, constrained by

$$\Gamma_{\rm I}(\boldsymbol{k};\eta) = \Gamma_{\rm I}(-\boldsymbol{k};-\eta) \quad \text{(S6)}$$

due to time-reversal symmetry (or, equivalently, $C^{s'}_{2z}$), parameterizes the impact of the Ising spin-orbit coupling in the band-projected theory. For momenta $\boldsymbol{k}$ where the mirror-even and mirror-odd bands of the trilayer system are energetically well separated, we have $\Gamma_{\rm I}(\boldsymbol{k};\eta) \approx \lambda_{\rm I}/2$ (using the conventions of [1, 3]), since the mirror-off-diagonal matrix elements of the Ising spin-orbit coupling only have a minor impact.

To simplify the form of Eq. (S5), let us perform the following transformation,

$$f_{\boldsymbol{k},\eta,s} \quad \longrightarrow \quad \left(e^{-i\frac{\varphi_\eta(\boldsymbol{k})}{2}\eta s_y}\right)_{s,s'} f_{\boldsymbol{k},\eta,s'} \quad \text{(S7)}$$

of the field operators. Choosing $\varphi_\eta(\boldsymbol{k}) = \arctan(B_x/\Gamma_{\rm I}(\boldsymbol{k};\eta))$, we absorb the impact of the magnetic field in Eq. (S5) by a rescaling of the Ising spin-orbit term,

$$H_{\rm LE} \longrightarrow \sum_{\boldsymbol{k},s,\eta} f^\dagger_{\boldsymbol{k},\eta,s} \left(\epsilon_{\eta\cdot\boldsymbol{k}} + \sqrt{\Gamma^2_{\rm I}(\boldsymbol{k};\eta) + B_x^2}\;(s_z)_{s,s'}\,\eta\right) f_{\boldsymbol{k},\eta,s'} + \sum_{\boldsymbol{k}} \left[f^\dagger_{\boldsymbol{k},+,s}(\Delta'_{\boldsymbol{k}})_{s,s'} f^\dagger_{-\boldsymbol{k},-,s'} + \text{H.c.}\right] + \delta H'_{\rm LE}. \quad \text{(S8)}$$

This already shows that the impact of the in-plane Zeeman field on the bandstructure and Fermi surfaces is rather different from that of the "conventional Rashba term" $(k_y s_x - k_x s_y)$ studied in [4–6, 8, 9]: instead of shifting Fermi surfaces in opposite directions, we can see that $B_x \neq 0$ only rescales the Ising spin-orbit coupling strength. As such, for each state at momentum $\boldsymbol{k}$ in valley η there has to be another state with the same energy at momentum $-\boldsymbol{k}$ in valley $-\eta$ and no finite momentum pairing is expected. Furthermore, there will be no diode effect since $C^{s'}_{2z}$ is still a symmetry. In fact, from a symmetry point of view, this conclusion is equivalent to the absence of a diode effect documented in Table SII for $S_{x,y}$ order and $\lambda_R = 0$, since S_x in Eq. (S3) and B_x in Eq. (S5) transform the same way under all symmetries of the system.

Note, however, that $B_x \neq 0$ does affect the spin-polarization of the Bloch states at the Fermi surface, an effect that becomes significant if B_x is of order of $\lambda_{\rm I}/2$. The accurate value of $\lambda_{\rm I}$ for our sample is not known, but we expect it to be in the range $\lambda_{\rm I}/2 \approx 0.5 - 5\,\text{meV}$ [3, 11]. This corresponds to a magnetic field strength of order of or larger than 8 T. From Eq. (S7) and using Eq. (S6), it follows that turning on B_x can be understood as a, in general $\boldsymbol{k}$ dependent, $\text{SU}(2)_+{\times}\text{SU}(2)_- \simeq \text{SO}(4)$ transformation of the singlet and triplet component,

$$\begin{pmatrix} \Delta^s_{\boldsymbol{k}} \\ d^x_{\boldsymbol{k}} \\ d^y_{\boldsymbol{k}} \\ d^z_{\boldsymbol{k}} \end{pmatrix} \quad \longrightarrow \quad \begin{pmatrix} \cos\varphi_+(\boldsymbol{k}) & 0 & i\sin\varphi_+(\boldsymbol{k}) & 0 \\ 0 & 1 & 0 & 0 \\ i\sin\varphi_+(\boldsymbol{k}) & 0 & \cos\varphi_+(\boldsymbol{k}) & 0 \\ 0 & 0 & 0 & 1 \end{pmatrix} \begin{pmatrix} \Delta^s_{\boldsymbol{k}} \\ d^x_{\boldsymbol{k}} \\ d^y_{\boldsymbol{k}} \\ d^z_{\boldsymbol{k}} \end{pmatrix}. \quad \text{(S9)}$$

This shows that, for instance, a finite singlet component $\Delta^s_{\boldsymbol{k}}$ at $B_x = 0$ will smoothly "rotate into" a $d^y_{\boldsymbol{k}}$ component with relative phase i when B_x is turned on. Note that even a $\text{SU}(2)_+{\times}\text{SU}(2)_-$ symmetric interaction $\delta H'_{\rm LE}$ will not be invariant under a $\boldsymbol{k}$-dependent transformation (S7), leading to $\delta H'_{\rm LE} \neq \delta H_{\rm LE}$. If, however, for the for superconductivity relevant parts of the MBZ $\Gamma_{\rm I}(\boldsymbol{k};\eta) \approx$ const. is a good approximation, we will have $\varphi_\eta(\boldsymbol{k}) \approx \varphi$ and, thus, $\delta H'_{\rm LE} \approx \delta H_{\rm LE}$ for any $\text{SU}(2)_+{\times}\text{SU}(2)_-$ symmetric interaction. Apart from the likely irrelevant impact of the rescaling $\lambda_{\rm R} \to \sqrt{\lambda^2_{\rm R} + (2B_x)^2}$, the critical temperature of superconductivity is (approximately) not affected by an in-plane Zeeman field, which can explain the Pauli-limit violation seen in Fig. S7d. Eventually, superconductivity will be suppressed by the in-plane orbital coupling associated with Peierls phases in the intralayer hopping [12].

Note that in-plane orbital coupling alone cannot induce a diode effect either: as can be seen in Table SI, the system exhibits the mirror symmetry σ_h as long as $D_0 = 0$ and in the absence of spin-orbit coupling. Since the in-plane orbital coupling is odd under σ_h, it is even under $\Theta\sigma_h$ which thus remain unbroken. Since the current, in turn, is odd under $\Theta\sigma_h$, Eq. (S2) holds, proving that an in-plane orbital coupling cannot induce a diode effect either in twisted trilayer graphene (as opposed to twisted bilayer graphene where this should be possible by symmetry [4]).

SI 3: Superconductivity in tTLG/WSe_2 heterostructures with different twist angle

TABLE SIII. We list material properties of five mirror-symmetric twisted trilayer graphene samples investigated in this work, such as twist angle and proximity with a WSe_2 crystal [3]. Superconductivity is observed in all the samples except sample E with a twist angle of $\theta = 1.38°$. In sample A, C and E, a few-layer WSe_2 crystal is stacked on top of tTLG, whereas tTLG in sample B and D are fully encapculated by hexagonal boron nitride crystals and the heterestructures do not contain WSe_2.

Sample	θ	WSe_2	T_c (K)	zero-field superconducting diode effect
A	$1.25° \pm 0.01°$	✓	1	✓
B	$1.31° \pm 0.01°$	✗	0.9	✓
C	$1.47° \pm 0.02°$	✓	1.4	✗
D	$1.50° \pm 0.02°$	✗	1.9	✗
E	$1.38° \pm 0.01°$	✓	0 (no superconductivity)	-

TABLE SIV. We summarize the main observations of different twist angle regimes. The twist angle dependence of flavor polarization and linear-in-T behavior is discussed in Ref. [3].

	Near the magic angle	small twist angle regime
Superconductivity	✓	✓
Flavor polarization	✓	✗
Linear-in-T behavior	✓	✗
Zero-field superconducting diode effect	✗	✓

SI 4: Longitudinal and transverse resistance in the normal state

We here discuss the connection between the observed non-trivial temperature dependence of R_{xy}/R_{xx} and the symmetries of the system. Let $\sigma_{\alpha,\beta}$, $\alpha,\beta = x,y$, be the conductivity tensor, which defines the relation between the in-plane current I_α and electric field E_α according to $J_\alpha = \sum_{\beta=x,y}\sigma_{\alpha,\beta}E_\beta$. We emphasize that the system has, as opposed to twisted bilayer graphene, no in-plane rotational symmetry (nor any mirror plane perpendicular to the graphene sheets) such that there is no specific in-plane high-symmetry direction that defines a natural orientation of our coordinates x and y. We parametrize σ as

$$\sigma = \begin{pmatrix} \sigma_0 & 0 \\ 0 & \sigma_0 \end{pmatrix} + \begin{pmatrix} 0 & \sigma_H \\ -\sigma_H & 0 \end{pmatrix} + \begin{pmatrix} \delta\sigma_0 & -\sigma_1 \\ -\sigma_1 & -\delta\sigma_0 \end{pmatrix}, \tag{S10}$$

where σ_H is only non-zero if time-reversal symmetry (more precisely Θ in Table SI combined with any spin-rotation) is broken, e.g., as a consequence of the valley-Hall effect discussed in the main text; furthermore, σ_1 and $\delta\sigma_0$ can only be non-zero if C_{3z} is broken.

Without loss of generality, let us assume that the x axis is chosen along the direction of the applied current in experiment. We then have $R_{xx} = (\sigma^{-1})_{x,x}$ and $R_{xy} = (\sigma^{-1})_{y,x}$. From this it is easy to see that

$$R_{xy}/R_{xx} = \frac{\sigma_H}{\sigma_0} \tag{S11}$$

in the case of broken Θ and preserved C_{3z} (e.g., valley polarization), while

$$R_{xy}/R_{xx} = \frac{\sigma_1}{\sigma_0 - \delta\sigma_0} \tag{S12}$$

if C_{3z} is broken but Θ preserved, as is the case in the presence of nematicity. Either way, R_{xy} is only non-zero if C_{3z} or Θ (or both) is (are) broken.

One crucial difference between the two scenarios is that R_{xy} will be isotropic, i.e., invariant under an in-plane rotation of the applied current and measured voltage if it results from broken Θ, while exhibiting a sinusoidal dependence on the rotation angle in the case of a nematicity-driving origin. As such, measuring R_{xy} or the ratio R_{xy}/R_{xx} as a function of this angle in future experiments will allow to determine its primary origin.

Finally, we comment on the finite and approximately constant value of R_{xy}/R_{xx} at higher temperatures, see in Fig. 3e-f. This can result from admixture of R_{xx} into R_{xy}, e.g., due to a slight misalignment of the voltage probes. It is often modeled [12] by an additional artificial contribution to R_{xy} that is proportional to R_{xx}, with prefactor that is independent of temperature; this can reproduce precisely the additional temperature-independent part in R_{xy}/R_{xx} that we observe at higher temperatures.

SI 5: the influence of proximity effect in sample A

The influence of the proximity effect in sample A is reflected by the following observations. The superconducting phase occupies an area in the $n-D$ map which spans the range of displacement field $-800 < D < 800$ mV/nm (Fig. 1c). According to this map, the superconducting phase exhibits a unique D dependence, which is not symmetric under $D \to -D$ at fixed ν_{tTLG}, but roughly invariant when the sign of both D and ν_{tTLG} is flipped. This D-dependence is further illustrated by examining the D-dependence in the optimal doping of the superconducting phase (Fig. **??**). The asymmetry in D demonstrates the influence of the WSe_2 crystal, which is present on only one side of tTLG and, hence, breaks the mirror (and inversion) symmetry of tTLG; the symmetry under $(D, \nu_{tTLG}) \to (-D, -\nu_{tTLG})$ is expected based on the bandstructure of the system [3]. The observed D-dependence not only highlights the influence of the tTLG/WSe_2 interface on the band structure but also on the interacting physics, including superconductivity. Despite the interfacial effect, R_{xx} as a function of T exhibits a sharp transition with critical temperature of $T_c \approx 1$ K, as can be seen in Fig. 1d. The sharp transition is consistent with the excellent sample quality with uniform twist angle.

SI 6: Density modulation in sample A

The interplay between DW instability and the stability of the superconducting phase has important implications for understanding the tTLG/WSe_2 heterostructure. There are two types of interplay, which are observed at different portions of the phase space: (i) at $D = 0$, as shown in Fig. 3a and Fig. 4a, the stability of the superconducting phase, reflected by quantities such as T_c and I_c, exhibits density modulation of 1/4 moiré filling; (ii) at $D = 325$ mV/nm, both T_c and I_c vary smoothly with ν_{tTLG} without any obvious density modulation. This is true even in the presence of the diverging DOS associated with DW instability. A natural explanation for both of these behaviors is that Cooper pair and DW instabilities compete against each other. As such, a weak superconducting phase exhibts density modulation, whereas a more robust one shows no modulation. We want to draw a clear distinction with the scenario that is discussed in Ref. [3], where the 2 and 4 unit cell states could potentially arise from a 4-fold enlarged moiré supercell, which is incuded by twist angle mismatch. In this scenario, superconductivity would be expected to exhibit a density modulation with 1/4 filling periodicity throughout the phase space. This scenario is inconsistent with our observations.

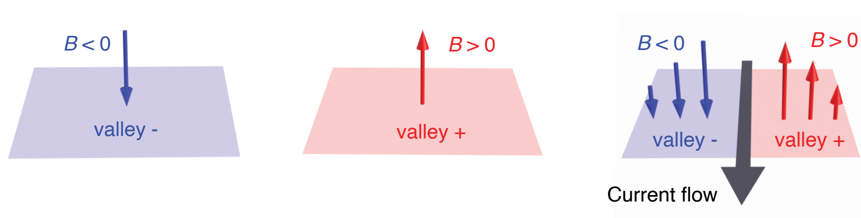

FIG. S1. **Schematics showing a possible mechanism underlying the influence of a large DC current.** As discussed in Ref. [1], the sign of partial valley imbalance in the underlying fermi surface can be trained using an external magnetic field in the presence of proximity induced SOC. This trainability provides the basis of our hypothesis that a large DC current untrains the diode effect by generating domains. Graphene moiré samples are known to exhibit varying degrees of twist angle inhomogeneity, which could give rise to inhomogeneous distribution of current flow across the sample. In this scenario, a large enough DC current flow could induce a local magnetic field profile which has opposite signs on two sides of the current path. At large DC bias, the current-induced field may be strong enough to stabilize opposite domains. Combined with a spatially inhomogeneous current distribution, this process could, in theory, untrain the superconducting diode effect.

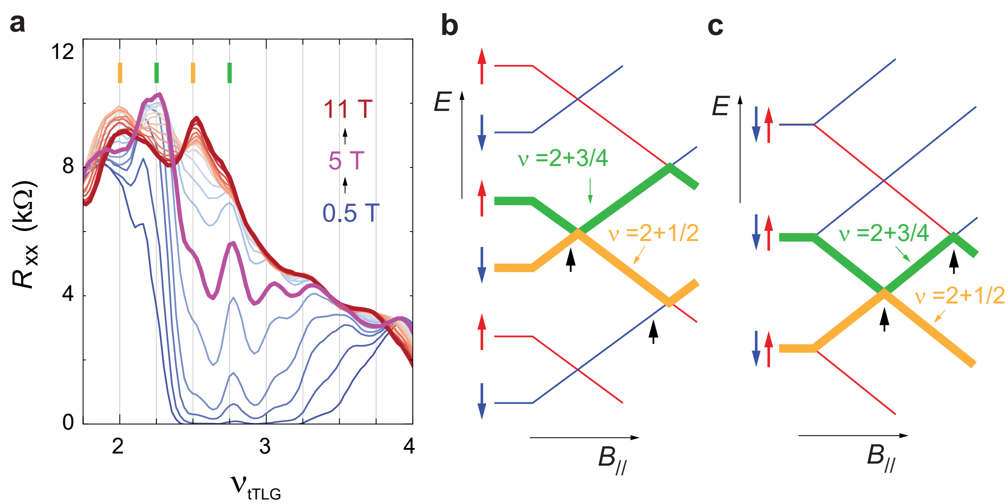

FIG. S2. **In-plane B dependence of density wave states.** (a) R_{xx} as a function of ν_{tTLG} measured at different $B_{\|}$. The vertical yellow and green bars mark DW states at every 1/4 fillings which exhibit different B-dependence. (b-c) Band diagram of DW states as a function of in-plane magnetic field. The observation in (a) is consistent with two possibilities: (b) DW sub-bands have alternating spin polarizations at $B_{\|} = 0$; (c) Sub-bands are realigned to be spin degenerate by Cooper pairing instability. The spin degeneracy is lifted by the application of $B_{\|}$. Although DW states appear at every 1/4 filling when superconductivity is suppressed by an out-of-plane magnetic field, an in-plane B-field gives rise to a doubling in the underlying degeneracy at $B_{\|}= 5$ and 11 T, where DW appears at every 1/2 moiré filling, as shown in (a). At $\nu_{tTLG} = 2+1/4$ and $2+3/4$, resistance peaks are robust at $B_{\|} \approx 5$ T but become suppressed by a large in-plane Zeeman coupling; on the other hand, the DW at $\nu_{tTLG} = 2$ and 2.5 are missing around $B_{\|}\approx 5$ T appear only at a large enough in-plane magnetic field of $B_{\|}\approx 10$ T. This unique $B_{\|}$-dependence points towards the possibility that the energy sub-band of DW states features alternating spin polarization. With increasing in-plane Zeeman field, sub-bands with opposite spin index cross at $B_{\|}\approx 5$ and 11 T (b), resulting in a doubling in degeneracy. If the DW states are the parent/normal state for superconductivity, the spin configuration of the superconducting phase is ill-defined. To reconcile these seemingly contradicting observations, the structure of energy sub-bands must be re-arranged at the onset of Cooper pairing instability. As a result, the band structure at $B = 0$ and $T = 0$ is different from $T > T_c$, or $B > B_c$. One possibility for the re-arranged band structure is shown in (c), where sub-bands with opposite spin polarization become degenerate so that each band is spin unpolarized at $B_{\|}= 0$. Although it is important to note that other band arrangements are possible as well.

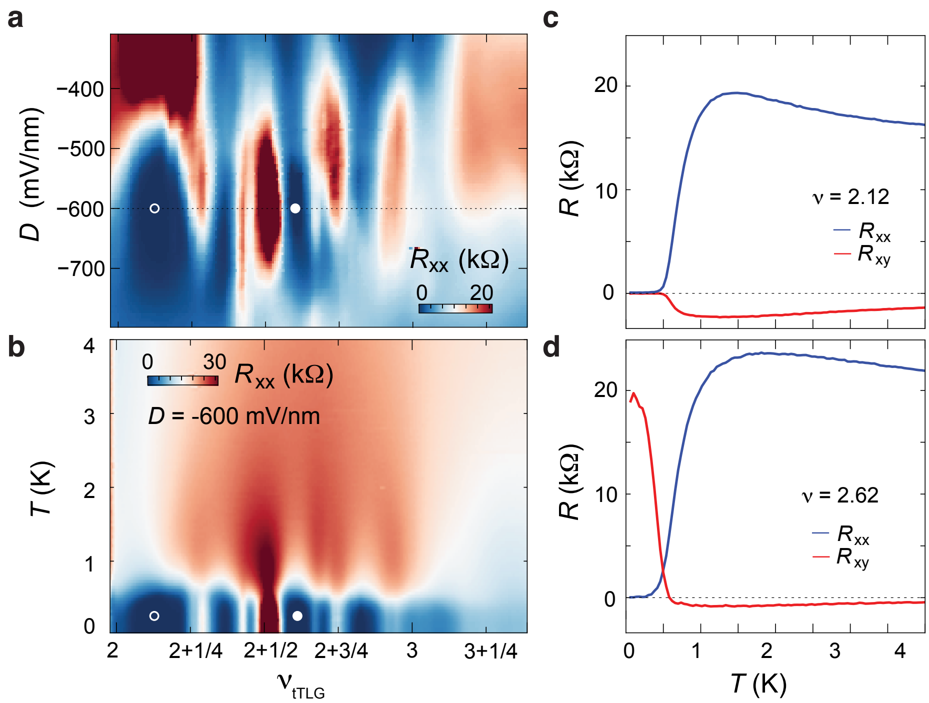

FIG. S3. **Transport anisotropy near $D = -600$ mV/nm.** (a) $\nu_{tTLG} - D$ map of R_{xx} measured at $B = 0$ and $T = 20$ mK. In this portion of the phase space, DW and superconductivity coexist at base temperature. (b) $\nu_{tTLG} - T$ map of R_{xx} measured at $B = 0$ and $D = -600$ mV/nm. (c) and (d) Temperature dependence of R_{xx} and R_{xy} measured at two positions marked by open and solid white circles in (a). Measurements are performed at $B = 0$ and $D = -600$ mV/nm. (c) At $\nu_{tTLG} = 2.12$, both R_{xx} and R_{xy} diminish at $T < T_c$. (d) At $\nu_{tTLG} = 2.62$, as R_{xx} diminishes with decreasing temperature, R_{xy} exhibits a sharp onset. At base temperature, the superconducting phase features a large robust Hall resistance. As alluded to in the main text, one possible origin of the strongly enhanced R_{xy} is spatial coexistence with the DW state. Due to the coexistence, superconducting transport naturally inherits the spatial anisotropy of the DW phase [3].

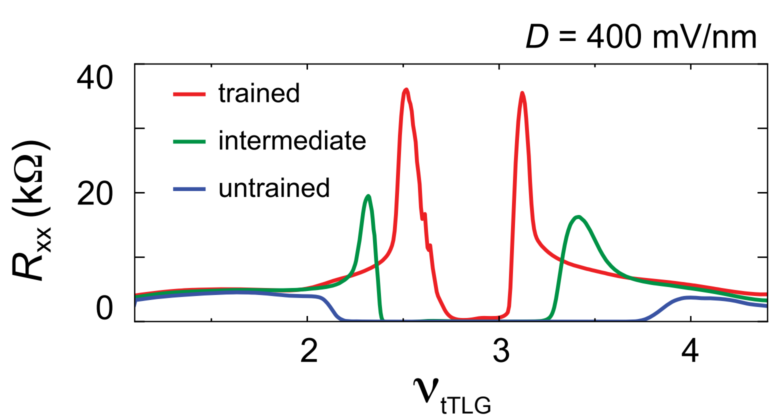

FIG. S4. R_{xx} **as a function of** ν_{tTLG} **for different field training conditions.** The red trace is measured after field training, where a robust superconducting diode effect is observed. The blue trace is measured after "untraining" using a large DC current, where $\Delta I_c \approx 0$. The green trace shows an intermediate configuration, where the nonreciprocity is present but not as robust as the fully "trained" configuration. All data is measured at $B = 0$, $T = 20$ mK and $D = 400$ mV/nm.

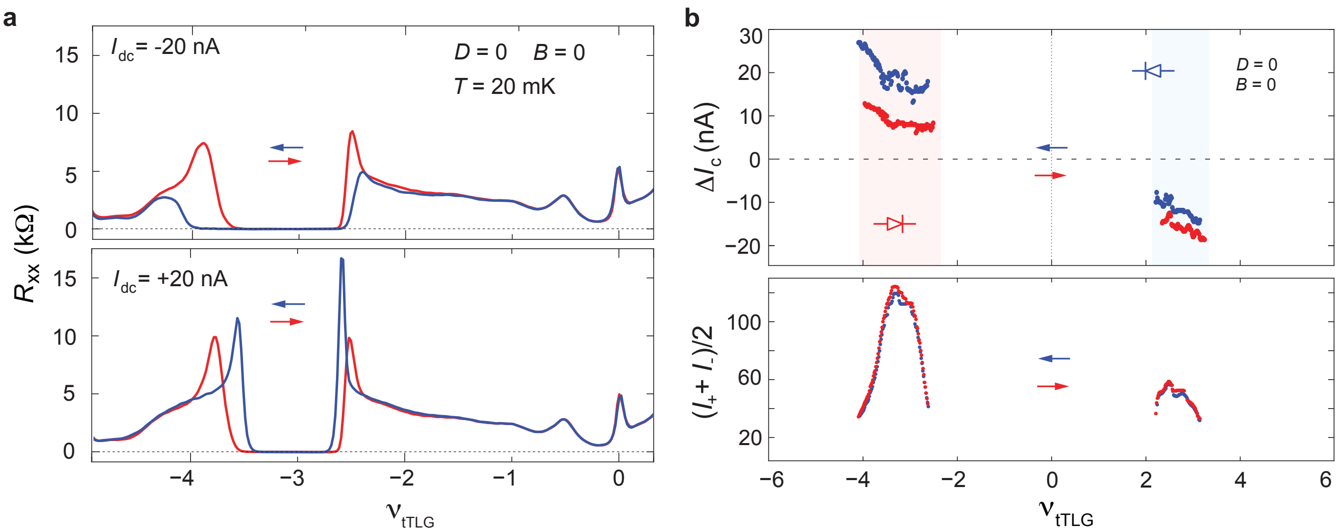

FIG. S5. **Hysteresis induced by field-effect doping in sample A.** (a) R_{xx} as a function of ν_{tTLG} measured with $I_{dc} = -20$ nA (top panel) and $+20$ nA (bottom panel). The red and blue traces are measured as carrier density is swept up and down, respectively. (b) ΔI_c (top panel) and $(I_c^+ + I_c^-)/2$ as a function of ν_{tTLG} as the density is swept back and forth. According to (a), the superconducting phase occupies different density ranges depending on the direction of sweeping filed-effect doping. This gives rise to a hysteretic transition between the superconducting-normal phases, which reflects the fact that zero-field nonreciprocity is dependent on the direction of sweeping field-effect doping. This is further demonstrated in (b), where the magnitude of ΔI_c is shown to be dependent on the direction of sweeping carrier density, even though the robustness of the superconductor, defined as $(I_c^+ + I_c^-)/2$, remains the same.

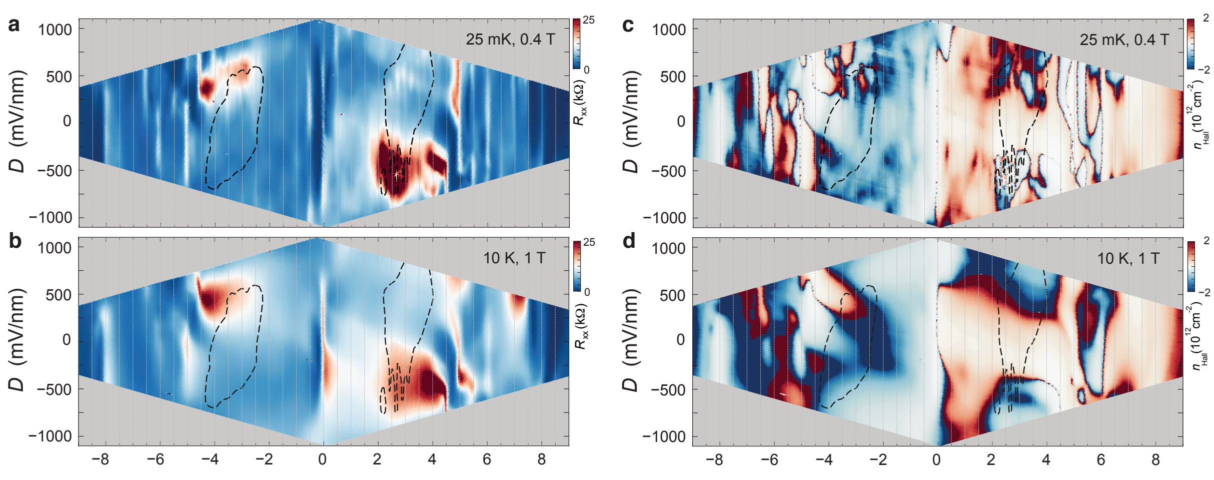

FIG. S6. **Longitudinal resistance and hall density at 20 mK and 10 K.** (a-b) Full range longitudinal resistance $\nu_{tTLG} - D$ map at (a) $T = 20$ mK, $B = 0.4$ T and (b) $T = 10$ K, $B = 1$ T. (c-d) Full range hall density $\nu_{tTLG} - D$ map at (c) $T = 20$ mK, $B = 0.4$ T and (d) $T = 10$ K, $B = 1$ T. The dashed lines outline the region of superconductivity.

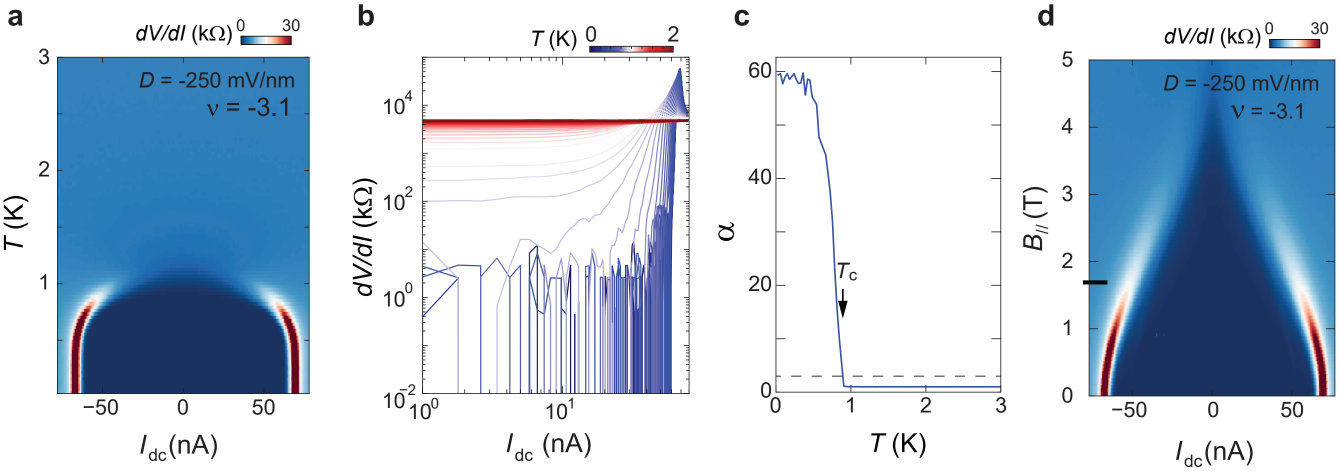

FIG. S7. **Pauli-limit breaking** (a) Differential resistance as a function of temperature and current, measured at $D = -250$ mV/nm and $\nu = -3.1$. (b) Log-log plot of differential resistance versus current at different temperatures. Data taken from (a). (c) α as a function of temperature, where α is the exponent in $V = I^{\alpha}$. α is extracted by adding one to the slope of the linear region in (b), which is defined by the first ten data points above the noise floor. Critical temperature $T_c = 0.9K$ is determined as the K-T transition temperature where $\alpha = 3$ (horizontal dashed line). (d) Differential resistance as a function of parallel magnetic field and current, measured at the same D and ν as (a). The black bar marks the Pauli-limit $B_{//} = 1.86T/K \times T_c$ for weakly coupled BCS superconductors [13, 14]. Here the superconductivity clearly violates the Pauli-limit as the critical parallel field exceeds the black bar.

[1] Scammell, H. D., Li, J. & Scheurer, M. S. Theory of zero-field superconducting diode effect in twisted trilayer graphene. *2D Materials* **9**, 025027 (2022).

[2] Christos, M., Sachdev, S. & Scheurer, M. S. Correlated insulators, semimetals, and superconductivity in twisted trilayer graphene. *Physical Review X* **12**, 021018 (2022).

[3] Siriviboon, P. *et al.* Abundance of density wave phases in twisted trilayer graphene on WSe_2. *arXiv e-prints* (2021). arXiv:2112.07127.

[4] Yuan, N. F. & Fu, L. Supercurrent diode effect and finite-momentum superconductors. *Proceedings of the National Academy of Sciences* **119**, e2119548119 (2022).

[5] Daido, A., Ikeda, Y. & Yanase, Y. Intrinsic superconducting diode effect. *Physical Review Letters* **128**, 037001 (2022).

[6] He, J. J., Tanaka, Y. & Nagaosa, N. A phenomenological theory of superconductor diodes. *New Journal of Physics* **24**, 053014 (2022).

[7] Ando, F. *et al.* Observation of superconducting diode effect. *Nature* **584**, 373–376 (2020).

[8] Agterberg, D. F. & Kaur, R. P. Magnetic-field-induced helical and stripe phases in Rashba superconductors. *Phys. Rev. B* **75**, 064511 (2007).

[9] Dimitrova, O. & Feigel'man, M. V. Theory of a two-dimensional superconductor with broken inversion symmetry. *Phys. Rev. B* **76**, 014522 (2007).

[10] Scheurer, M. S. & Samajdar, R. Pairing in graphene-based moiré superlattices. *Phys. Rev. Research* **2**, 033062 (2020).

[11] Naimer, T., Zollner, K., Gmitra, M. & Fabian, J. Twist-angle dependent proximity induced spin-orbit coupling in graphene/transition metal dichalcogenide heterostructures. *Physical Review B* **104**, 195156 (2021).

[12] Cao, Y. *et al.* Nematicity and competing orders in superconducting magic-angle graphene. *Science* **372**, 264–271 (2021).

[13] Chandrasekhar, B. A note on the maximum critical field of high-field superconductors. *Applied Physics Letters* **1**, 7–8 (1962).

[14] Clogston, A. M. Upper limit for the critical field in hard superconductors. *Physical Review Letters* **9**, 266 (1962).